INTERNATIONAL JOURNAL FOR NUMERICAL METHODS IN FLUIDS, VOL. 20, 935–955 (1995)

MULTIDIMENSIONAL UPWINDING: ITS RELATION TO FINITE ELEMENTS

J.-C. CARETTE, H. DECONINCK AND H. PAILLERE

von Karman Institute for Fluid Dynamics, Chaussée de Waterloo 72, B-1640 Rhode-Saint-Genèse, Belgium

AND

P. L. ROE

The University of Michigan, Ann Arbor, MI 48109-2140, U.S.A.

SUMMARY

Vertex-based multidimensional upwind schemes for scalar advection are compared with shock-capturing SUPG finite element methods based on linear triangular elements. Both methods share the same compact stencil and are formulated as cell-wise residual distribution methods. The distribution for the finite element method is 1/3, supplemented with a Lax–Wendrov-type dissipation term, while the distribution for the upwind schemes is limited to the downstream nodes of the element. The multidimensional upwind schemes use positivity as the monotonicity criterion, while the finite element method includes a residual-based non-linear dissipation.

For hyperbolic systems such as the compressible Euler equations the upwind method relies on a multidimensional wave model to decompose the residual into scalar contributions. From this observation a new SUPG formulation for systems is proposed in which the scalar SUPG method is applied to each of the decomposed residuals obtained from the wave model, thereby providing a better-founded definition of the τ dissipation matrix and shock-capturing term in the SUPG methods.

KEY WORDS SUPG finite element method; multidimensional upwinding; cell vertex advection schemes; Euler equations

1. INTRODUCTION

Finite element methods for advection-dominated partial differential equations have now reached a high level of maturity based on many new developments over the last decade.[1–3] These include the introduction of the SUPG test function for scalar advection[4] to avoid contamination of the entire solution by spurious oscillations arising for the standard Galerkin method in the underresolved parts of the domain; addition of residual-based non-linear artificial dissipation[2,5] to suppress oscillations remaining in underresolved domains; and finally the extension of these two concepts to systems by construction of an SUPG dissipation τ-matrix and generalized discontinuity-capturing terms.[6–8]

Both the SUPG test function and the non-linear dissipation are well understood and mathematically founded for a scalar advection–diffusion equation, while it is well recognized that the extension to systems with non-commuting Jacobians is still heuristic. It is precisely the goal of this paper to contribute in this respect by proposing the wave-modelling tool developed in the context of multidimensional upwind schemes as a way of extending scalar SUPG to systems.

Multidimensional vertex-based upwind methods on triangles have been developed during the last 5 years in a joint effort between the University of Michigan and the von Karman Institute; see References 9–13 for a detailed account. In a first phase, scalar advection schemes on triangles (or tetrahedra in 3D)

CCC 0271–2091/95/090935–21

have been constructed based on the principle of residual distribution (or fluctuation splitting).[10] For each triangle the residual is evaluated and subsequently distributed over the vertices with weighting coefficients summing to unity. It turns out that by limiting the distribution to the downstream vertices only, i.e. creating upwind schemes, the schemes can be made positive by construction, thus ensuring monotonic discontinuity capturing. Adding the constraint of linearity preservation, which is equivalent to the residual property in finite elements, is impossible unless one introduces non-linearity in the schemes (even when solving a linear advection equation). This is similar to what occurs with the TVD schemes in the finite volume setting. In this way, compact non-linear high-resolution upwind advection schemes on triangles have been developed which are positive by construction. The most recent development was a reformulation of these non-linear schemes using classical limiter functions such as the minmod function.[13]

Since these upwind schemes share the same compact stencil as finite element schemes on linear triangles, it is natural to present them in the same framework and to compare their performances, which is the second goal of this paper. The SUPG schemes for scalar advection can be written as a central distribution (1/3) with additional Lax–Wendrov-type dissipation.[10,14] An order-of-accuracy study on a smooth test case (with solution fully resolved by the mesh) reveals second-order accuracy for linear SUPG and the linear (non-monotonic) upwind advection scheme termed LDA, while the non-linear schemes on the same test case show an order of accuracy of 1·6, both for the shock-capturing SUPG and the non-linear upwind scheme termed PSI.[15] On test cases with underresolved layers the non-linear upwind scheme is slightly less diffusive than the optimally tuned shock-capturing SUPG scheme.

As mentioned before, the application of the scalar advection upwind schemes to non-diagonalizable systems such as the Euler equations for compressible flow needs as a prerequisite a device, called a wave model, which decomposes the system residual into a set of scalar contributions, each associated with a well-defined advection direction and speed. Many such wave models have been proposed over the last years with some degree of success[11] and the subject is certainly not fully mature. However, over the last year it has been recognized that the key property of a wave model is the linear independence of the eigenvectors onto which the residual is projected. Only in this way is one assured that a vanishing system residual will result in vanishing contributions of each scalar component. This effectively rules out some of the early wave models based on a number of (linearly dependent) simple waves.[16]

In this paper we focus on recent models[13,17] which satisfy this property. They use the Mach lines and streamline as propagation directions in supersonic flow and an algebraic extension (the pseudo-Mach lines) together with the streamline in subsonic flow.

Once a satisfactory wave model is available, it is very natural and tempting to use it as well in the context of the SUPG finite element methods by applying the scalar SUPG test function and shock-capturing term to each of the decomposed residuals given by the model. In this way, some of the heuristics in the system extension of SUPG is removed as well. The computational results presented in this paper show the potential of this approach.

2. SCALAR ADVECTION

Fluctuation splitting or residual distribution is a cell vertex space discretization for the scalar advection equation

$$u_t + \vec{\lambda} \cdot \vec{\nabla} u = 0, \tag{1}$$

where $\vec{\lambda}$ is the advection vector, which depends on the space co-ordinates and eventually on the solution itself. For simplicity, let it be constant; see e.g. Reference 10 for the non-linear case and for

conservation aspects. The solution is approximated by a continuous piecewise linear representation on triangles,

$$u(x,y,t) = \sum_i u_i(t) w_i(x,y), \tag{2}$$

where u_i is the point value $u(x_i, y_i)$ and $w_i(x, y)$ is the standard linear finite element basis function. For a given triangulation of the domain the residual or 'fluctuation' for each triangle T with surface S_T can be computed as

$$\phi_T = \int\int_T \frac{\partial u}{\partial t} \mathrm{d}S = -S_T \vec{\lambda} \cdot \vec{\nabla} u = -\sum_{i=1}^{3} u_i k_i, \tag{3}$$

where

$$k_i = S_T \vec{\lambda} \cdot \vec{\nabla} w_i = \tfrac{1}{2} \vec{\lambda} \cdot \vec{n}_i \tag{4}$$

and $\vec{n}_i$ is the inward normal of the side E_i opposed to node i, scaled by the length of E_i. Considering simple Euler explicit time integration, all residual distribution schemes can be cast into the following compact form for mesh point i:

$$u_i^{n+1} = u_i^n + \frac{\Delta t}{S_i} \sum_T \beta_{T,i} \phi_T, \tag{5}$$

where the summation extends over all triangles having i as common vertex, $\beta_{T,i}$ is the so-called distribution coefficient and S_i is the area of the *median dual cell* around node i. For conservation and consistency the coefficients $\beta_{T,i}$ are chosen such that for each triangle T with vertices j, $\sum_{j=1}^{3} \beta_{T,j} = 1$. For compactness of the stencil the restriction is made to consider only the distribution of the fluctuation ϕ_T within the triangle T.

Referring to Reference 10, three essential design criteria can be imposed on a distribution scheme, namely continuity, positivity ($\mathscr{P}$) and linearity preservation ($\mathscr{LP}$). Continuity requires that the distribution coefficients $\beta_{T,i}$ be at least continuous for changes in advection speed $\vec{\lambda}$ as well as for changes in the solution. Positivity means that every new value u_i^{n+1} can be written as a convex combination of values at time level n. This guarantees a maximum principle which prohibits the occurrence of new extrema and ensures stability of the explicit scheme (5). Linearity preservation or exactness for linear polynomials requires that the scheme preserve the exact steady state solution when this is a linear function of the space co-ordinates x and y for an arbitrary triangulation of the domain. This is known as the residual property in the finite element context. A necessary and sufficient condition for a scheme to be $\mathscr{LP}$ is that the distribution coefficients $\beta_{T,i}$ be bounded for $\phi_T \to 0$.

The residual can be distributed to the nodes of a triangle in many ways and well-known schemes can be identified in this framework. We briefly review some of these schemes and give the residual distribution interpretation of SUPG.

2.1. *Upwind fluctuation-splitting schemes*

Upwind fluctuation-splitting schemes are upwind in the sense that no contribution is sent to upstream nodes. This can be expressed as

$$\beta_{T,i} = 0 \quad \text{if } k_i < 0. \tag{6}$$

Figure 1 shows the two possible situations that can occur in a triangle. In case (a) there is only one inflow side and the entire fluctuation is sent to the unique downstream node 3, while in case (b) the fluctuation is split between the two downstream nodes 1 and 3. Both positive and linearity-preserving

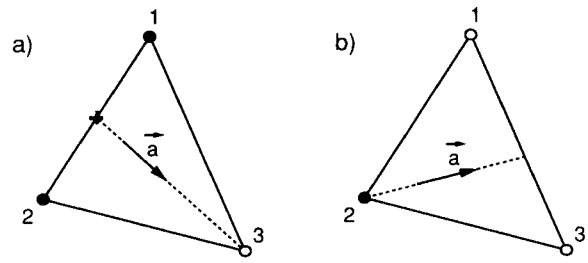

Figure 1. (a) One-target situation. (b) Two-target situation

schemes have been developed. To combine the two properties, it has been proven that the schemes have to be made non-linear.[10]

A straightforward linear $\mathscr{LP}$ scheme is the LDA scheme given by[18]

$$\beta_{T,i}^{LDA} = \frac{\max(0,k_i)}{\sum_{j=1}^{3} \max(0,k_j)}. \tag{7}$$

The linear positive (but therefore not $\mathscr{LP}$) scheme with lowest dissipation is the N scheme given by

$$\beta_{T,i}^{N} = \frac{\phi_i}{\phi_T}, \tag{8}$$

where

$$\phi_i = -\frac{\max(0,k_i)}{\sum_{l=1}^{3} \max(0,k_l)} \sum_{j=1}^{3} \min(0,k_j)(u_i - u_j). \tag{9}$$

It is easy to verify that this scheme is positive; however, it is not $\mathscr{LP}$ since the $\lim_{\Phi_T \to 0} |\beta_{T,i}^{N}|$ is not bounded.

A non-linear scheme combining positivity and linearity preservation is the PSI scheme.[12,19] Recently[13] it has been found that this non-linear scheme can be written as a limited version of the N scheme, namely as

$$\beta_{T,i}^{PSI} = \Psi(\beta_{T,i}^{N}) = \Psi\left(\frac{\phi_i}{\phi_T}\right), \tag{10}$$

where $\Psi(r)$ is the well-known minmod limiter

$$\Psi(r) = \max(0, \min(r, 1)). \tag{11}$$

One verifies that applying the limiter does not destroy positivity, but it bounds the coefficient β between zero and one, rendering the scheme $\mathscr{LP}$.

Summarizing, both the LDA and PSI schemes have the continuity and $\mathscr{LP}$ properties. In addition, the PSI scheme is positive under a CFL condition, unlike the LDA scheme.

2.2. *Fluctuation-splitting interpretation of the Lax–Wendrov scheme*

To obtain the distribution coefficients for a Lax–Wendrov scheme, let us write, to second order,

$$u^{n+1} - u^n \approx \Delta t\, u_t + \tfrac{1}{2}\Delta t^2 u_{tt} = -\Delta t \vec{\lambda} \cdot \vec{\nabla} u - \tfrac{1}{2}\Delta t^2 \vec{\lambda} \cdot \vec{\nabla} u_t. \tag{12}$$

Integrating now over the median dual cell area S_i relative to node i and lumping the LHS leads to an equidistribution supplemented with a dissipation term proportional to an edge-wise CFL number:[14]

$$\beta_{T,i}^{LW} = \frac{1}{3} + \frac{1}{2}\Delta t \frac{k_i}{S_T}. \tag{13}$$

2.3. *Fluctuation-splitting interpretation of SUPG*

For the classical Galerkin finite element method it can easily be shown that the distribution coefficient is $\beta_{T,i}^{\text{Gal}} = \frac{1}{3}$, which is not surprising since this method is known to be a central-type discretization.

Hughes' version of SUPG makes use of asymmetric test functions of the form

$$\tilde{w}_i = w_i + \tau_1 \vec{\lambda} \cdot \vec{\nabla} w_i + \tau_2 \vec{\lambda}_{\|} \cdot \vec{\nabla} w_i, \tag{14}$$

where the first term is the standard Galerkin test function, the second term is the linear SUPG modification and the third term is the non-linear discontinuity-capturing dissipation. The vector $\vec{\lambda}_{\|}$ is the projection of the advection vector $\vec{\lambda}$ onto the direction of the local gradient of the solution, and τ_1 and τ_2 are two parameters defined as follows in a pure advection context:

$$\tau_1 = \frac{1}{2}\frac{h}{|\vec{\lambda}|}, \qquad \tau_2 = \frac{1}{2}\frac{h}{|\vec{\lambda}_{\|}|}, \tag{15}$$

h being the size of the discretization. The distribution coefficients for this method have been obtained in Reference 19 and take the form

$$\beta_{T,i}^{\text{SUPG Hughes}} = \tfrac{1}{3} + \tau_1 \frac{k_i}{S_T} + \tau_2 \frac{(k_i)_{\|}}{S_T}. \tag{16}$$

where $(k_i)_{\|} = \frac{1}{2}\vec{\lambda}_{\|} \cdot \vec{n}_i$ is defined as k_i but using the $\vec{\lambda}_{\|}$-field. For $\tau_1 = \frac{1}{2}\Delta t$ and $\tau_2 = 0$ this scheme reduces precisely to the Lax–Wendrov scheme of Section 2.2, while with $\tau_1 = 0$ and $\tau_2 = \frac{1}{2}\Delta t$ we have a Lax–Wendrov scheme based on the advection speed $\vec{\lambda}_{\|}$.

While Hughes introduces the so-called discontinuity-capturing term in the test function itself, Johnson uses an artificial viscosity $\hat{\kappa}$.[2] The modified equation solved when using $\hat{\kappa}$ is

$$u_t + \vec{\lambda} \cdot \vec{\nabla} u - \vec{\nabla} \cdot (\hat{\kappa} \vec{\nabla} u) = 0. \tag{17}$$

The SUPG test function considered is as (14) but without the non-linear term. To derive the distribution coefficients, we use a simplified form of the artificial viscosity proposed by Johnson[2] and given by

$$\hat{\kappa} = \frac{1}{2} h \frac{|\vec{\lambda} \cdot \vec{\nabla} u|}{|\vec{\nabla} u| + h}. \tag{18}$$

More precisely, the jump term which is usually added to the residual in the numerator of $\hat{\kappa}$ is neglected. This simplification is acceptable since this jump term has been experimented numerically to be of very small effect in the computations. With this simplification the distribution coefficients take the form

$$\beta_{T,i}^{\text{SUPG Johnson}} = \frac{1}{3} + \tau \frac{k_i}{S_T} + \frac{1}{2} h \frac{|\vec{\nabla} u|}{|\vec{\lambda} \cdot \vec{\nabla} u|} \frac{(k_i)_{\|}}{S_T}. \tag{19}$$

Now, since $|\vec{\lambda}_{\|}| = |\vec{\lambda} \cdot \vec{\nabla} u| / |\vec{\nabla} u|$, the distribution coefficients of Johnson's and Hughes' versions of SUPG appear to be the same, which confirms the well-known equivalence of these two versions for a pure advection equation with constant advection vector.

2.4. *Numerical results for scalar advection*

Order of accuracy at steady state. In Reference 15 an accuracy study was performed to estimate the order of different advection schemes for smooth solutions resolved by the mesh. The definition of the problem considered for this study was proposed by Struijs.[12] The computational domain is the unit square $\Omega = [-1, 0] \times [0, 1]$. The advection speed vector is $\vec{\lambda} = (y, -x)$ which corresponds to a clockwise rotation around the origin, while the boundary conditions are $u = 0$ at the right boundary and $u = \frac{1}{2}e^{-2x}[1 - \cos(2\pi x)]$ at the lower boundary.

Using the L_2-norm, the following schemes have been compared: the N, LDA and PSI schemes, Johnson's version of SUPG without artificial viscosity (SUPG) and with artificial viscosity (SUPG + AV). Table I summarizes the orders of accuracy as well as the properties they satisfy.

A first observation is that the introduction of a non-linear artificial viscosity decreases the order of accuracy of SUPG. This is the price one has to pay for increasing the robustness of SUPG in the presence of sharp layers. This is also the case for the non-linear PSI scheme compared with the linear LDA scheme. The value of 1·99 for linear SUPG is better than that predicted by theory,[20] since global error estimates for smooth solutions give an accuracy $\mathcal{O}(k + \frac{1}{2})$ with a polynomial of degree k. However, this theoretical value must be taken as a minimum. Indeed, numerical studies performed by Nävert[21] suggest that linear SUPG has an accuracy $\mathcal{O}(k + 1)$ in many cases in which the exact solution is sufficiently smooth, which is confirmed by Hughes[1] and our results. There is a strong similarity in performance for both the two linear $\mathscr{LP}$ and the two non-linear $\mathscr{LP}$ schemes.

Rotational advection of a square profile. Consider now a linear advection problem in which a square profile imposed at the inflow boundary is rotationally advected over the domain $[-1, 1] \times [0, 1]$. The advection speed vector is $\vec{\lambda} = (y, -x)$ and the boundary conditions are

$$\begin{cases} u(x,0) = 0 & \text{if } -1{\cdot}00 < x < -0{\cdot}65, \\ u(x,0) = 1 & \text{if } -0{\cdot}65 < x < -0{\cdot}35, \\ u(x,0) = 0 & \text{if } -0{\cdot}35 < x < 0{\cdot}00, \\ u(-1,x) = 0 & \text{if } 0{\cdot}00 < y < 1{\cdot}00, \\ u(x,1) = 0 & \text{if } 0{\cdot}00 < x < 1{\cdot}00. \end{cases}$$

The exact steady state solution is $u = 1$ in between the two half-circles with radii 0·35 and 0·65 and $u = 0$ elsewhere. The mesh used is regular and isotropic, with 61 nodes in the x-direction and 31 nodes in the y-direction, giving a total of 1891 nodes and 3600 elements. The mesh and the isolines of the steady state solutions are depicted in Figure 2. The SUPG method and the LDA scheme are both non-monotonic and produce very similar oscillatory solutions. The SUPG + AV method shows a monotonic solution but does not perform as well as the PSI scheme. Indeed, the introduction of the artificial viscosity cancels the over- and undershoots but increases the crosswind diffusion. In all cases the square profile spreads out in the streamwise direction. Since the characteristics propagate parallel to the discontinuities themselves, there is nothing to counteract this diffusive effect.

Table I. Properties and order of accuracy for different fluctuation-splitting and SUPG schemes

Scheme	Non-linear	Positive	Property $\mathscr{LP}$	Order of accuracy
N	No	Yes	No	0·83
LDA	No	No	Yes	1·95
PSI	Yes	Yes	Yes	1·65
SUPG	No	No	Yes	1·99
SUPG + AV	Yes	No	Yes	1·63

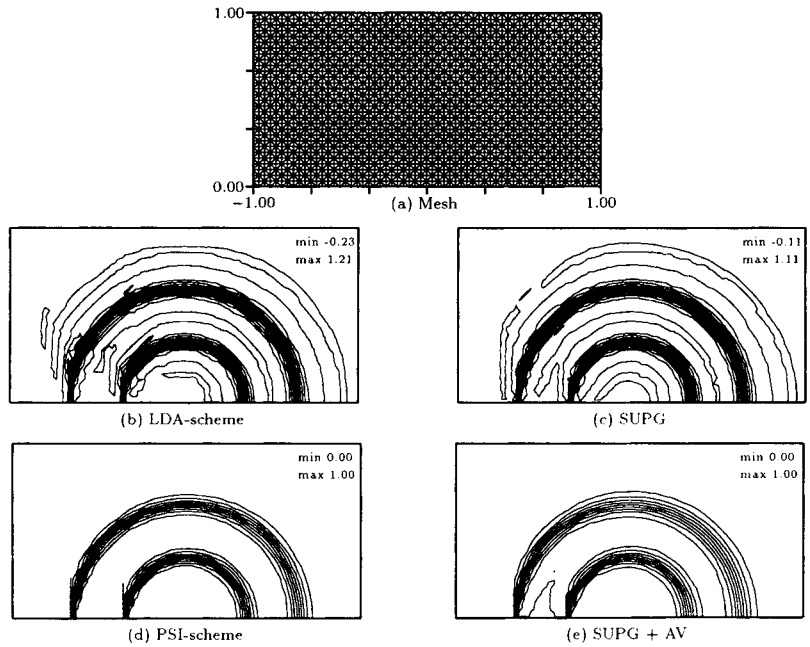

Figure 2. Rotational advection of a square profile: mesh and contour lines

3. EULER EQUATIONS

The Euler equations in conservative form are

$$\mathbf{U}_t + \mathbf{F}_x + \mathbf{G}_y = 0, \tag{20}$$

where $\mathbf{U}$ is the vector of conservation variables and $\mathbf{F}$ and $\mathbf{G}$ are the flux vectors:

$$\mathbf{U} = \begin{pmatrix} \rho \\ \rho u \\ \rho v \\ \rho E \end{pmatrix} \qquad \mathbf{F} = \begin{pmatrix} \rho u \\ \rho u^2 + p \\ \rho uv \\ \rho uH \end{pmatrix} \qquad \mathbf{G} = \begin{pmatrix} \rho v \\ \rho uv \\ \rho v^2 + p \\ \rho vH \end{pmatrix}. \tag{21}$$

Here ρ is the density of the gas, u and v are the x- and y-components of the velocity vector $\vec{u}$, respectively, p is the static pressure, E is the specific total energy and $H = E + p/\rho$ is the specific total enthalpy. The system is closed by the equation of state, which in the case of a perfect gas may be written as

$$p = (\gamma - 1)\rho[E - \tfrac{1}{2}(u^2 + v^2)], \tag{22}$$

with γ the ratio of specific heats. We denote the speed of sound by $a = \sqrt{(\gamma p/\rho)}$.

For a system of equations the fluctuation-splitting schemes are based on an eigenvector decomposition of the residual in each cell, which then allows the application of the scalar advection scheme to each component.

In one dimension the solution gradient of the Euler equations can be projected uniquely onto the eigenvectors $\mathbf{r}^k$ of the Jacobian matrix $\mathbf{A} = \partial\mathbf{F}/\partial\mathbf{U}$, leading to the decomposition of the flux divergence $\mathbf{F}_x$ into waves or 'characteristics' travelling along the axis. In 2D the waves can travel in an infinite number of directions. The decomposition of the flux divergence into scalar waves is therefore no longer unique. At present three different approaches exist which are compared in References 11 and

17. The first approach is based on characteristic compatibility equations of the Euler system,[22] the second on a simple wave decomposition of the solution[16,23] and the third on a projection of the solution onto a basis of steady and unsteady patterns.[24] Here only the two first approaches are considered, namely the characteristic decomposition technique and the simple wave decomposition.

3.1. Simple wave decomposition

Simple wave decomposition relies on a 'pattern recognition' step whereby the local flow gradients are modelled by contributions of a set of simple waves. Simple waves are elementary solutions of the Euler equations for linearly varying flow of the form

$$\mathbf{U}(\vec{x}, t) = \alpha(\vec{x} \cdot \vec{m} - \lambda_m t)\mathbf{r} + \mathbf{U}_0 = [W(\vec{x}, t) + W_0]\mathbf{r}, \tag{23}$$

where α and $\vec{m} = \cos\theta\vec{1}_x + \sin\theta\vec{1}_y$ are constants representing the wave strength and the direction of propagation of the wave front respectively; λ_m and $\mathbf{r}$ are the corresponding eigenvalues and right eigenvector of the matrix $(\partial\mathbf{F}/\partial\mathbf{U})\cos\theta + (\partial\mathbf{G}/\partial\mathbf{U})\sin\theta$ respectively. These eigenvalues, given as

$$\lambda_m^{a+} = \vec{u} \cdot \vec{m} + a, \tag{24a}$$

$$\lambda_m^{a-} = \vec{u} \cdot \vec{m} - a, \tag{24b}$$

$$\lambda_m^{s} = \vec{u} \cdot \vec{m}, \tag{24c}$$

$$\lambda_m^{e} = \vec{u} \cdot \vec{m}, \tag{24d}$$

are the wave speeds of two acoustic waves, a shear wave and an entropy wave respectively, while the right eigenvectors in the primitive variables $(\rho, u, v, p)^{\mathrm{T}}$ are given by

$$\mathbf{r}^{a\pm} = \begin{pmatrix} \rho/a \\ \pm\cos\theta^k \\ \pm\sin\theta^k \\ \rho a \end{pmatrix}, \qquad \mathbf{r}^{s} = \begin{pmatrix} 0 \\ -\sin\theta^k \\ \cos\theta^k \\ 0 \end{pmatrix}, \qquad \mathbf{r}^{e} = \begin{pmatrix} 1 \\ 0 \\ 0 \\ 0 \end{pmatrix}. \tag{25}$$

The scalar $W(\vec{x}, t)$ is a pseudocharacteristic variable evolving in time according to the scalar advection equation

$$W_t + \vec{\lambda} \cdot \vec{\nabla} W = 0, \tag{26}$$

where $\vec{\lambda}$ is such that $\vec{\lambda} \cdot \vec{m} = \lambda_m$. Assuming that the solution can be interpreted as the superposition of a discrete number K of simple waves, one has to solve for the strengths and directions of these waves to obtain a wave model. The requirement for a simple wave model is that it should have enough degrees of freedom to describe any arbitrary linear variation of the solution. Thus in 2D a wave model should have eight degrees of freedom (the eight components of the constant gradient) represented by the unknown directions and/or intensities. Ideally this requires a model composed of four simple waves, namely one entropy, one shear and two acoustic waves, the four directions and four intensities being the parameters of the model.

However, matching four such waves with a solution gradient leads to a non-linear system for the eight parameters which is far too complex to be useful. Therefore most models have been constructed with a larger basis of simple waves where some directions and intensities are fixed *a priori* on physical grounds.

Different models have been proposed following this approach.[16,23] For instance, the Mach-angle-splitting model, developed by Rudgyard[23] and valid for supersonic flows only, decomposes the gradient of the solution into seven waves: one entropy wave and two sets of waves each comprising two acoustic waves and one shear wave with propagation vector $\vec{m}$ normal to the Mach lines; see Figure 3. This gives a complete model since there are eight unknowns, i.e. the strength and direction of the

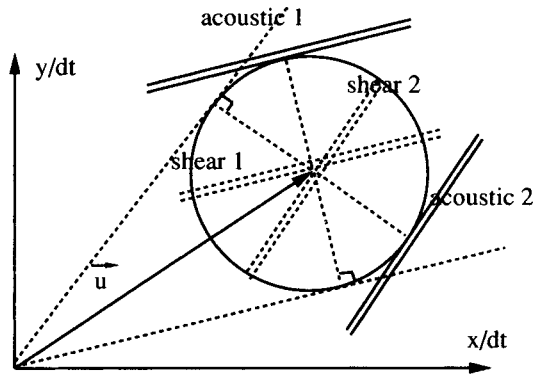

Figure 3. Wave directions for the Mach-angle-splitting model (entropy wave not represented)

entropy wave and the strengths of the four acoustic and two shear waves. Note that the choice of the directions normal to the Mach lines cancels the speeds of two acoustic waves, so that one is left with five effective waves contributing to the residual decomposition.

In conclusion, by selecting a simple wave model involving K active simple waves, the element-wise residual can be decomposed as

$$\Phi_T = \oint_{\partial T} (\mathbf{F}\mathrm{d}y - \mathbf{G}\mathrm{d}x) = -\sum_{k=0}^{K-1} (\vec{\lambda}^k \cdot \vec{\nabla} W^k)\mathbf{r}^k, \tag{27}$$

where W^k is the scalar 'pseudocharacteristic' variable and $\mathbf{r}^k$ is its corresponding right eigenvector in conservative variables.

3.2. *Characteristic decomposition*

Simple wave models as described in the previous subsection have the drawback that they are not $\mathscr{LP}$, since the eigenvectors are necessarily linearly dependent if the number of effective waves exceeds four. The approach considered here is therefore based on a selection of four independent compatibility equations.

Originally Deconinck *et al.*[22] proposed an approximate diagonalization procedure for the Euler equations based on a two-parameter similarity transformation. Here we consider a generalization of this approach towards a three-parameter similarity transformation[13,17] given by

$$\partial \mathbf{W} = \begin{pmatrix} \partial\rho - \partial p/a^2 \\ \vec{s}^{(1)} \cdot \partial\vec{u} \\ \frac{1}{2}(\vec{\kappa}^{(2)} \cdot \partial\vec{u} + \partial p/\rho a) \\ \frac{1}{2}(\vec{\kappa}^{(3)} \cdot \partial\vec{u} + \partial p/\rho a) \end{pmatrix} = \mathbf{P}^{*-1}\partial\mathbf{U}, \tag{28}$$

where $\mathbf{W}(\vec{\kappa}^{(1)}, \vec{\kappa}^{(2)}, \vec{\kappa}^{(3)})$ is a vector of characteristic variables, $\mathbf{U}$ is the vector of conservation variables, $\mathbf{P}^{*-1}$ is the transformation matrix from conservative to characteristic variables, $\vec{\kappa}^{(1)}$, $\vec{\kappa}^{(2)}$ and $\vec{\kappa}^{(3)}$ are three given vectors in x–y space, $\vec{s}^{(1)}$ is the vector perpendicular to $\vec{\kappa}^{(1)}$ and similarly for $\vec{s}^{(2)}$ and $\vec{s}^{(3)}$. Substituting into the Euler system (20), the following system of compatibility equations is obtained:

$$W_t^0 + \vec{u} \cdot \nabla W^0 + q^0 = 0, \tag{29a}$$

$$W_t^1 + \vec{u} \cdot \nabla W^1 + q^1 = 0, \tag{29b}$$

$$W_t^2 + (\vec{u} + a\vec{\kappa}^{(2)}) \cdot \nabla W^2 + q^2 = 0, \tag{29c}$$

$$W_t^3 + (\vec{u} + a\vec{\kappa}^{(3)}) \cdot \nabla W^3 + q^3 = 0, \tag{29d}$$

where the q^k are coupling terms of the form

$$q^0 = 0, \tag{30a}$$

$$q^1 = \vec{s}^{(1)} \cdot \nabla p/\rho, \tag{30b}$$

$$q^2 = \frac{a}{2}\vec{s}^{(2)} \cdot (\vec{s}^{(2)} \cdot \nabla)\vec{u}, \tag{30c}$$

$$q^3 = \frac{a}{2}\vec{s}^{(3)} \cdot (\vec{s}^{(3)} \cdot \nabla)\vec{u}, \tag{30d}$$

For certain choices of $\vec{\kappa}^{(1)}$, $\vec{\kappa}^{(2)}$ and $\vec{\kappa}^{(3)}$ one can obtain an optimal decoupling of the Euler system, since q^1 can be set to zero by choosing $\vec{\kappa}^{(1)}$ parallel to the pressure gradient and $q^2 = q^3$ can be minimized by choosing adequately $\vec{\kappa}^{(2)}$ and $\vec{\kappa}^{(3)}$. This was the approach followed in Reference 22, but it leads to gradient-dependent and therefore non-robust decompositions.

In the new formulation considered in References 13 and 17 the parameters are no longer chosen so as to minimize the off-diagonal terms appearing in the set of compatibility equations, but rather so as to express these compatibility equations in more physical directions.

For instance, by taking the vectors $\vec{\kappa}^{(1)}$ normal to the streamline and the vectors $\vec{\kappa}^{(2)}$ and $\vec{\kappa}^{(3)}$ normal to the two Mach lines which make angles $\pm\ \mu$ with the streamline,

$$\mu = \tan^{-1}\left(\frac{1}{\sqrt{(M^2-1)}}\right), \tag{31}$$

one obtains the optimal characteristic decomposition for steady supersonic flows, effectively upwinding the Riemann invariants of steady supersonic flow along their corresponding characteristics (see Reference 17 for more details).

This approach becomes ill-defined when $M \rightarrow 1^+$, because the steady equations become parabolic. Therefore, in order to avoid a singularity occurring at $M = 1$, we consider two splittings corresponding to the choices $\vec{\kappa}^{(1)} = \vec{\kappa}^{(2)} = -\vec{\kappa}^{(3)} = \vec{\kappa}_A$ and $\vec{\kappa}^{(1)} = \vec{\kappa}^{(2)} = -\vec{\kappa}^{(3)} = \vec{\kappa}_B$, where $\vec{\kappa}_A$ and $\vec{\kappa}_B$ are the normals to the Mach lines; see Figure 4. In order to extend this decomposition to subsonic flows, we consider an algebraic continuation of μ by defining a pseudo-Mach angle

$$\mu = \tan^{-1}\left(\frac{1}{\sqrt{|M^2-1|}}\right). \tag{32}$$

Averaging these two splittings gives a characteristic model called the pseudo-Mach angle (PMA) decomposition.[13] Figure 4 shows the different advection directions used. As can be seen, the model is continuous at the sonic point and always respects the domain of dependence of the steady flow as determined by the nature of the equations. In particular, when $M \rightarrow 0$, the decomposition becomes isotropic.

Summarizing, for the PMA decomposition the element-wise residual can be decomposed as

$$\Phi_T = -\frac{1}{2}\left(\sum_{k=0}^{3}(\vec{\lambda}^k\vec{\nabla}W^k + q^k)_{\vec{\kappa}_A}\mathbf{r}^k_{\vec{\kappa}_A} + \sum_{k=0}^{3}(\vec{\lambda}^k \cdot \vec{\nabla}W^k + q^k)_{\vec{\kappa}_B}\mathbf{r}^k_{\vec{\kappa}_B}\right), \tag{33}$$

with $\mathbf{r}^k$ the right eigenvectors appearing in the transformation matrix $\mathbf{P}^*$.

3.3. Multidimensional upwind schemes

Once an analytical simple wave model (for which $q^k = 0$, $\forall k$) or a characteristic decomposition has been chosen, the residual for each triangle is decomposed as

$$\oint_{\partial T}(\mathbf{F}dy - \mathbf{G}dx) = S_T\sum_{k=0}^{K-1}(\overline{\vec{\lambda}^k} \cdot \vec{\nabla}W^k)\mathbf{r}^k + \overline{q^k})\overline{\mathbf{r}^k}, \tag{34}$$

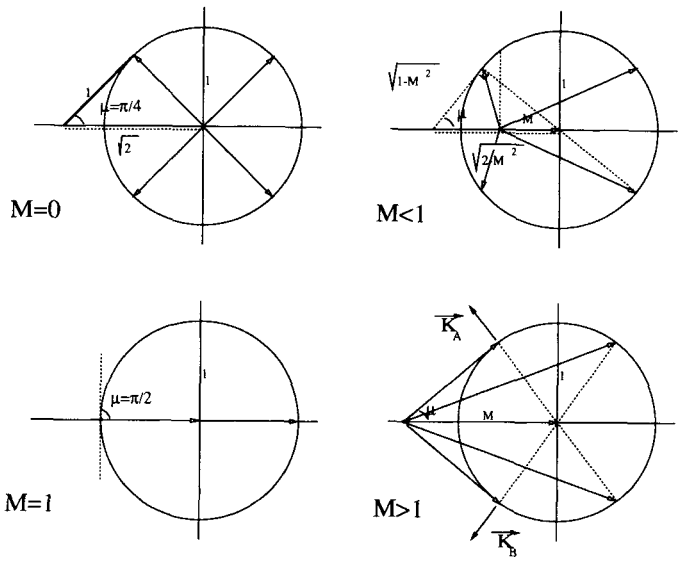

Figure 4. Upwinding directions for pseudo-Mach angle decomposition

where overlining denotes a suitable conservative linearization not discussed here.[25] Applying now a scalar advection scheme to each wave, the residual of each element can be distributed in a conservative way to the nodes. After performing the residual distribution step, the solution can be updated. The final update formula can be written as

$$\mathbf{U}_i^{n+1} = \mathbf{U}_i^n - \frac{\Delta t}{S_i} \sum_T \sum_{k=0}^{K-1} \beta_{T,i}^k S_T (\overline{\vec{\lambda}^k} \cdot \vec{\nabla} W^k + \overline{q^k}) \overline{\mathbf{r}^k}, \tag{35}$$

where the summation index T carries over all triangles having i as common vertex, while $\beta_{T,i}^k$ represents the fraction of the residual of the kth wave in element T sent to node i.

3.4. *Application of wave modelling to SUPG*

Despite all efforts undertaken, the key problem of extending scalar SUPG results to general hyperbolic systems, in particular to the inviscid compressible Euler equations, remains without definitive answer. Indeed, the construction of the τ stabilization matrix and the shock-capturing term is not a trivial task. It is only under severe restrictions such as those for one-dimensional and/or diagonalizable systems that one can find optimal definitions.[6,7] In these cases, different scalar SUPG test functions and non-linear dissipation can be used for each of the decoupled equations, each of them being optimal as in the case of a single scalar equation. For more complex cases, global generalizations have been defined based on approximate diagonalization or some privileged direction such as the streamlines or the normal to a discontinuity.[26] Here, as an alternative to such global approaches, it is proposed to introduce the wave-modelling technique which allows the use of the scalar formulation also in the general case.

Let us assume that we are equipped with a given simple wave model combining K waves (in which case $q^k = 0$, $\forall k$) or with a given characteristic decomposition. The element-wise residual of the 2D

Euler equations in their conservative form (20) can then be decomposed into K contributions as explained above:

$$\frac{\partial \mathbf{U}}{\partial t} = \sum_{k=0}^{K-1} \frac{\partial W^k}{\partial t} \mathbf{r}^k = -\sum_{k=0}^{K-1} (\vec{\lambda}^k \vec{\nabla} W^k + q^k) \mathbf{r}^k. \tag{36}$$

Each contribution is associated with a scalar advection equation in the (pseudo)characteristic variable W^k for which one can apply the SUPG scalar scheme. Using finite element methodology with piecewise linear functions in space, we thus have, for the scalar residual in node i due to wave k,

$$\phi_i^k = -\sum_{T \in \Omega_E} \int\int_T [\tilde{w}_i^k (\vec{\lambda}^k \vec{\nabla} W^k + q^k) + \hat{\kappa}^k \vec{\nabla} w_i \vec{\nabla} W^k] \mathrm{d}\Omega \tag{37}$$

where $\tilde{w}_i^k = w_i + \tau^k \vec{\lambda}^k \vec{\nabla} w_i$ is the standard SUPG test function. Note that the stability parameter τ and the artificial viscosity $\hat{\kappa}$ are defined for each individual scalar contribution:

$$\tau^k = \frac{h}{2|\vec{\lambda}^k|}, \qquad \hat{\kappa}^k = \frac{1}{2} \frac{h|\vec{\lambda}^k \vec{\nabla} W^k + q^k|}{|\vec{\nabla} W^k| + h}. \tag{38}$$

Thus the linear SUPG modification of the test functions is achieved for each wave in its own direction of propagation and the stability parameters τ^k are such that the amount of upstream biasing is controlled individually wave-by-wave. Moreover, the non-linear dissipation associated with a given wave has the property that it vanishes if the element-wise residual vanishes for that particular wave. Regrouping the K wave contributions, one obtains the global residual in conservation variables for node i,

$$\Phi_i = \sum_{k=0}^{K-1} \Phi_i^k = \sum_{k=0}^{K-1} \phi_i^k \mathbf{r}^k, \tag{39}$$

which can be written as

$$\Phi_i = -\sum_{T \in \Omega_E} \int\int_T \left(\sum_{k=0}^{K-1} [\tilde{w}_i^k (\vec{\lambda}^k \vec{\nabla} W^k + q^k) + \hat{\kappa}^k \vec{\nabla} w_i \vec{\nabla} W^k] \mathbf{r}^k \right) \mathrm{d}\Omega. \tag{40}$$

It is of particular interest to separate the SUPG and the artificial dissipation terms from the Galerkin term. Indeed, the exact decomposition of the flux divergence can then be isolated, which shows that the Galerkin term can be computed in the classical way, i.e. without using wave modelling.

The new formation for the compressible Euler equations presented here has the advantage of using only the scalar SUPG scheme for each component of the solution, which is well-defined and understood.

3.5. Numerical results

Different wave models and characteristic decompositions combined with either the fluctuation-splitting schemes or the SUPG method are tested and compared on a series of five test cases ranging from the low subsonic regime to hypersonic re-entry flow.

Supersonic parallel jet interaction. Two horizontal supersonic parallel jets separated by a wall are suddenly brought into contact.[27] The interaction of the two streams produces a shock wave propagating in the low-pressure region, a Prandtl–Meyer expansion propagating in the high-pressure region and a contact discontinuity in between the two. The computational domain [0, 1] × [0, 1] has been

discretized using a uniform isotropic grid with 41 × 41 nodes, giving a total of 1681 nodes and 3200 elements. All boundaries except the left were taken as supersonic outlets. At the left boundary, supersonic inlet boundary conditions have been specified:

$$\begin{cases} M_1 = 4{\cdot}00, \\ \rho_1 = 0{\cdot}50 \quad \text{if } y > 0{\cdot}5, \\ p_1 = 0{\cdot}25, \end{cases} \qquad \begin{cases} M_2 = 2{\cdot}40, \\ \rho_2 = 1{\cdot}00 \quad \text{if } y \leqslant 0{\cdot}5, \\ p_2 = 0{\cdot}50 \end{cases}$$

The density line contours are presented in Figure 5. The first solution has been obtained with the global SUPG formulation recently proposed by Hansbo[26] (SUPG C_A), while the other two have been produced by combining the PSI scheme and the SUPG scalar scheme respectively with the so-called Mach-angle-splitting model designed by Rudgyard[23] and valid for supersonic flows only. First of all note that the SUPG C_A method does not capture the contact discontinuity very well, while the PSI scheme and the SUPG method using wave modelling produce close solutions showing an excellent resolution of the three flow features. Solution (d) is slightly more diffusive, confirming the observations made for the scalar problems. This could be expected, since the only difference between these last two methods is the advection scheme they involve.

Supersonic wedge channel. The next test case consists of a supersonic flow at $M_\infty = 2{\cdot}0$ in a channel. To solve this problem, an unstructured mesh with 3987 nodes and 7683 elements was used, demonstrating the geometrical flexibility of the methods presently studied. The unstructured mesh (as

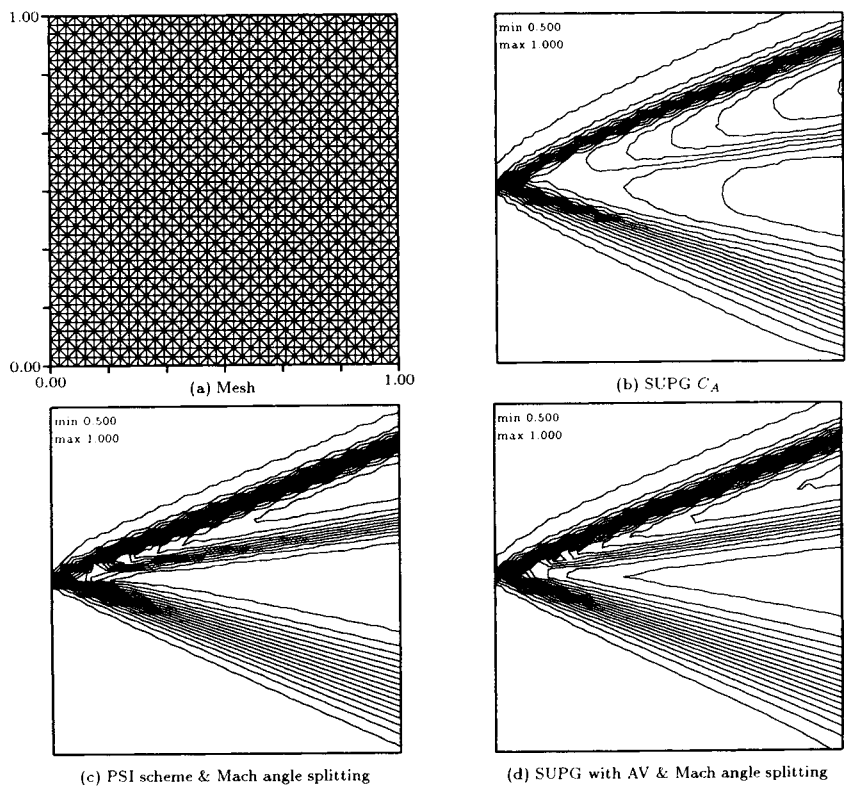

(a) Mesh (b) SUPG C_A

(c) PSI scheme & Mach angle splitting (d) SUPG with AV & Mach angle splitting

Figure 5. Parallel jet interaction: mesh and density line contours

well as the other unstructured meshes shown in the following) was generated using a frontal Delaunay method developed by Müller *et al.*[28] and by applying afterwards a weighted smoothing technique as proposed by Richter.[29] This technique, based on the spring analogy, alters the positions of the interior nodes, taking into account the degree of each node in order to better control the regularity without changing the topology of the grid.

Figure 6 shows the grid and the Mach number contours produced by the SUPG scheme with non-linear dissipation combined with Rudgyard's Mach-angle-splitting model, by the same scheme associated with the PMA decomposition and finally by the PSI scheme combined with the optimal characteristic decomposition for supersonic flow. All methods show very similar solutions with all features of the flow clearly resolved. They compare well with the solution obtained by Richter[29] with an Osher scheme on a $\pm$ 3 times finer grid. Note that the convex discontinuity of the lower wall creates a non-physical generation of entropy which is then advected parallel to the wall and increased through the successive shocks, influencing the flow downstream.

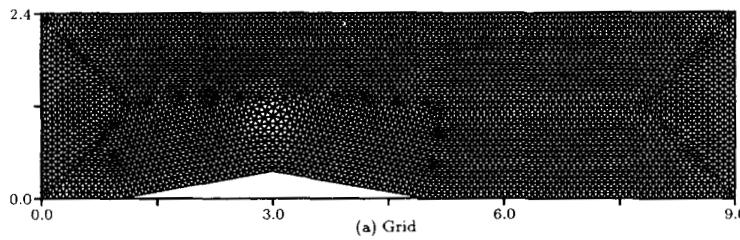

(a) Grid

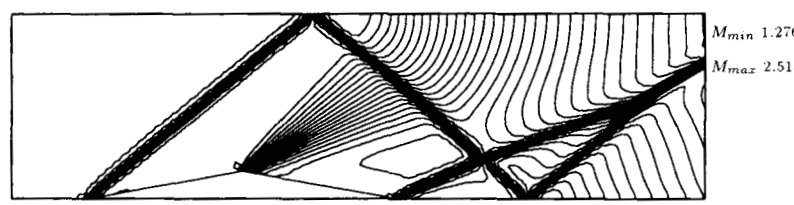

(b) SUPG with AV & Mach angle splitting

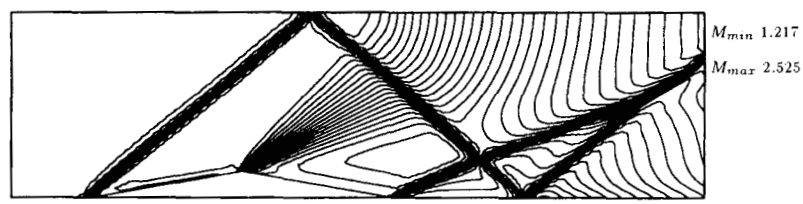

(c) SUPG with AV & PMA decomposition

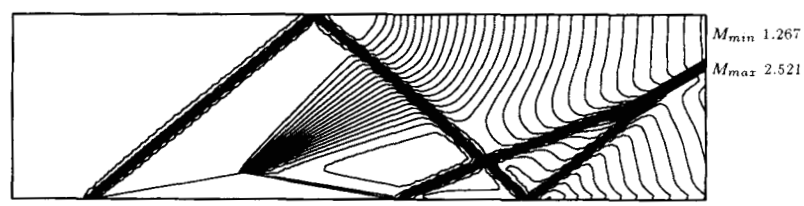

(d) PSI scheme & "optimal" decomposition

Figure 6. Supersonic wedge channel: mesh and Mach number line contours

Subcritical flow about a cylinder. The flow over a cylinder at $M_\infty = 0{\cdot}38$ is now considered. The mesh, shown in Figure 7, consists of 8471 triangular elements and 4330 nodes, with 128 nodes on the body and 60 nodes in the far field. The theoretical solution is a potential solution (irrotational and isentropic) with no lift and no drag. Four computations have been performed.

In the first two computations the pseudo-Mach angle decomposition was used in combination with the LDA scheme and the SUPG scheme without non-linear artificial viscosity, producing small values of lift and drag as given in Table II. The Mach number isolines are shown in Figures 8(a) and 8(b), confirming the high degree of symmetry of the solution with respect to the X- and Y-axes and showing very low levels of spurious entropy. These two solutions compare well with the best solutions obtained in Reference 30.

The third and fourth computations have been achieved using the simple wave model D (composed of six waves[31]) associated with the LDA scheme and the PMA decomposition associated with the SUPG scheme with non-linear dissipation. In the solution obtained with model D, which is not linearity-preserving, one can observe a large entropy error ($\Sigma_{max} = 0{\cdot}0996$) and consequently an increase in drag ($C_D = 0{\cdot}6760$) and a complete asymmetrization of the flow with respect to the Y-axis but a good symmetry of the flow with respect to the X-axis, resulting in a small value of lift ($C_L = 0{\cdot}000924$). Essentially the same (but not so dramatic) observations can be made about the solution produced by the SUPG scheme with non-linear dissipation. This test case shows clearly that non-linearity-preserving models (such as model D) have to be avoided as well as the use of non-linear artificial dissipation for the SUPG scheme when dealing with subcritical flows.

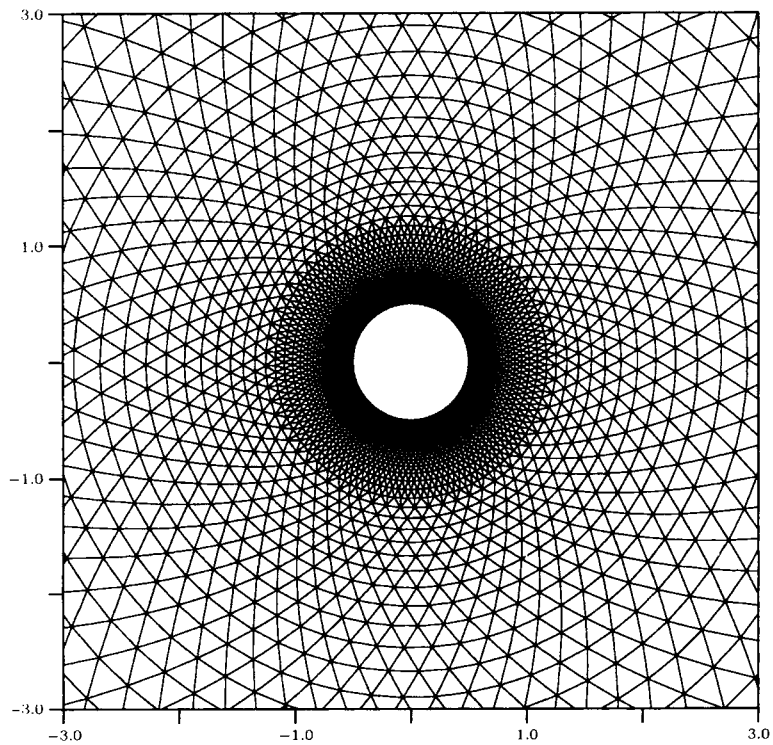

Figure 7. Cylinder $M_\infty = 0{\cdot}38$: detailed view of the grid

Table II. Cylinder $M_\infty = 0{\cdot}38$: values of C_L and C_D

Solution	Model	Scheme	C_L	C_D
(a)	PMA	LDA	−0·010689	0·000526
(b)	PMA	SUPG	0·006814	−0·001232
(c)	D	LDA	0·000924	0·676016
(d)	PMA	SUPG + AV	0·002084	0·324879

Subcritical multielement aerofoil. The flow field around a four-element aerofoil with freestream Mach number $M_\infty = 0{\cdot}2$ and zero angle of attack is computed using the PMA decomposition associated with the SUPG scheme without non-linear dissipation. Owing to the entropy generated in the successive stagnation regions and transported along the bodies, an additional non-standard dissipation has been necessary in the form of vorticity damping as used by Giles *et al.*[32] in order to counteract the grid line/velocity decoupling observed in the vicinity of the bodies.

The grid, a detail of which is shown in Figure 9, contains 10,018 elements and 5217 nodes, with the far field located at 15 chords. The Mach number isolines and the entropy contours are shown in Figures 10(a) and 10(b) respectively, while the pressure coefficient distributions along the bodies are shown in Figure 11.

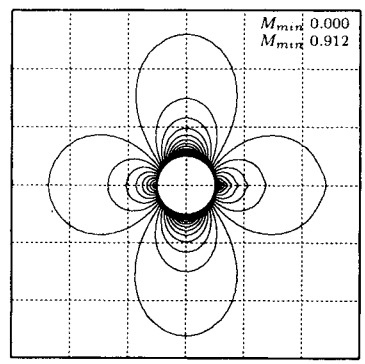

(a) Pseudo-Mach angle decomposition, LDA scheme

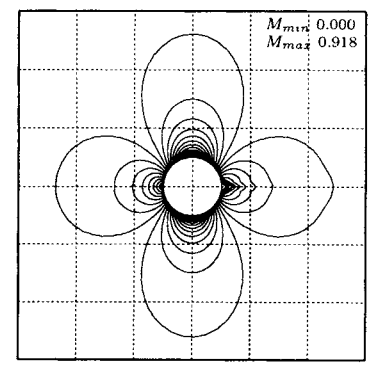

(b) Pseudo-Mach angle decomposition, SUPG scheme

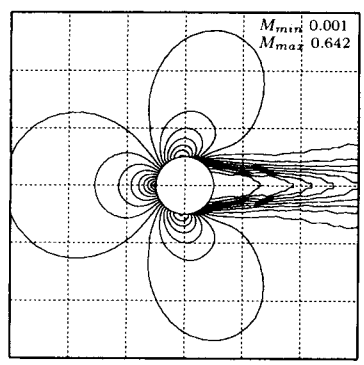

(c) Model D, LDA scheme

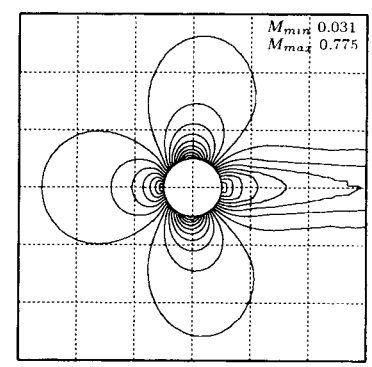

(d) Pseudo-Mach angle decomp., SUPG + AV scheme

Figure 8. Cylinder $M_\infty = 0{\cdot}38$: Mach number isolines

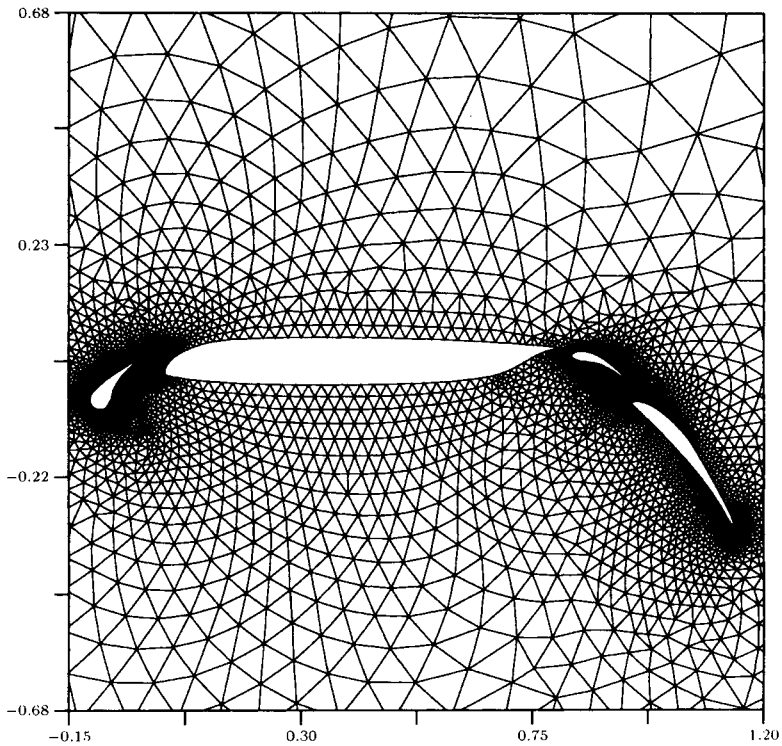

Figure 9. Multi-element airfoil: detailed view of the grid.

Hypersonic flow about a double ellipse. The next test case corresponds to the hypersonic flow about a double ellipse at $M_\infty = 8{\cdot}15$ and 30° angle of attack.[33] This flow is characterized by a strong bow shock in the front part and by a weaker shock generated at the canopy attachment point.

The grid shown in Figure 12 has 9823 elements and 5111 nodes, of which 195 are on the body. The computation has been performed by using the SUPG scheme with non-linear artificial dissipation associated with the PMA decomposition.

The Mach number isolines of the solution are depicted in Figure 13(a), while the pressure isolines are shown in Figure 13(b). Figure 14 displays the pressure coefficient distribution along the body. All these compare well with the solutions presented in Reference 33.

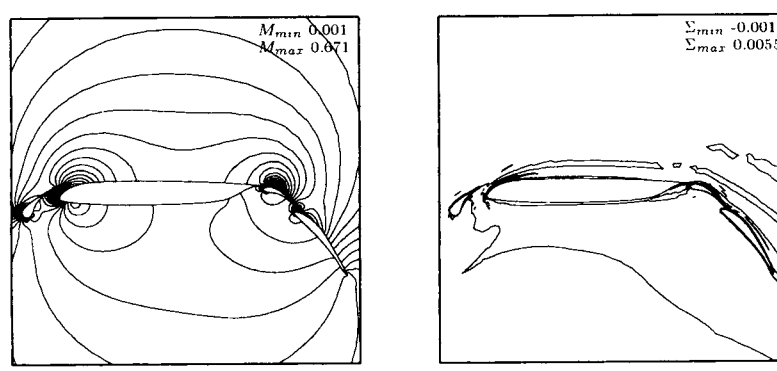

(a) Mach number isolines (b) Entropy isolines

Figure 10. Multielement aerofoil: $M_\infty = 0{\cdot}2$, $\alpha = 0°$

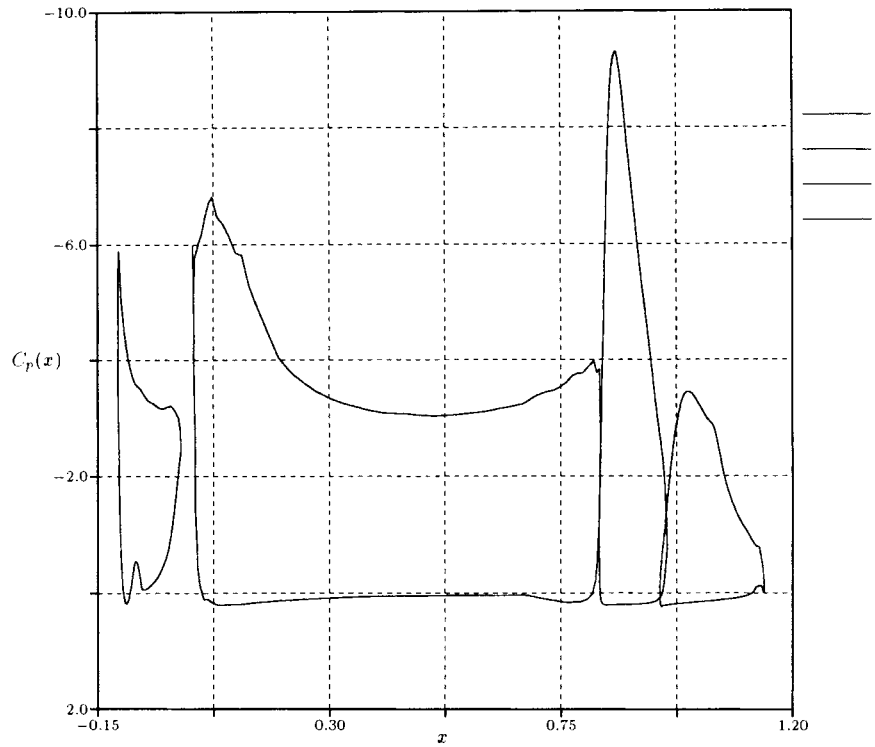

Figure 11. Multielement aerofoil: pressure coefficient distributions along the bodies

4. CONCLUSIONS

Scalar SUPG shock-capturing finite element schemes have been formulated as residual distribution schemes and compared with multidimensional upwind schemes sharing the same compact stencil. Wave modelling, which is essential to extend the multidimensional scalar upwind schemes towards systems, turns out to be advantageous in the SUPG finite element context as well, leading to a systematic approach for generalizing the scalar formulation.

ACKNOWLEDGEMENTS

The first two authors strongly acknowledge Professor T. Hughes for his suggestion to investigate the use of wave models for extending scalar SUPG to the system case. Part of this research has been supported by the Hermes Research on Qualification programme under contract ALG 91/13 monitored by Dassault Aviation. J.-C. C. is a Ph.D. candidate financially supported by a Belgian government IRSIA fellowship.

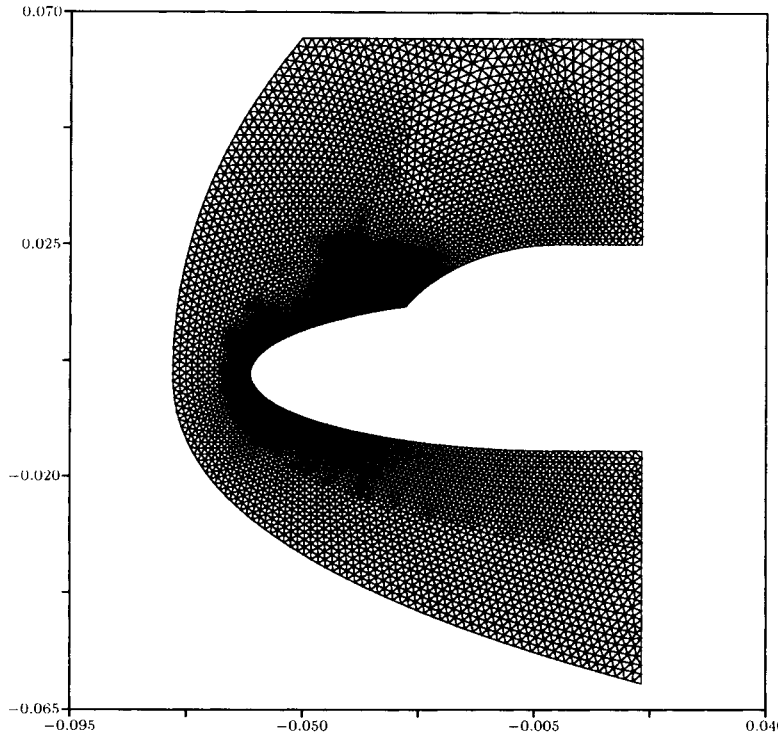

Figure 12. Double ellipse: grid

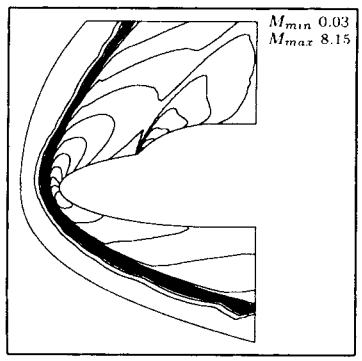

(a) Mach number isolines

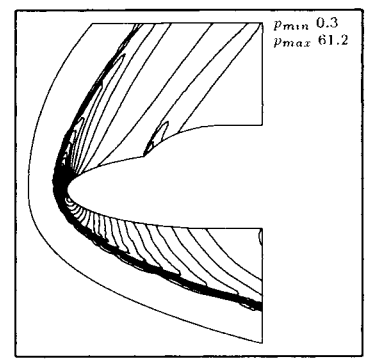

(b) Pressure isolines

Figure 13. Double ellipse: $M_\infty = 8{\cdot}15$, $\alpha = 30°$

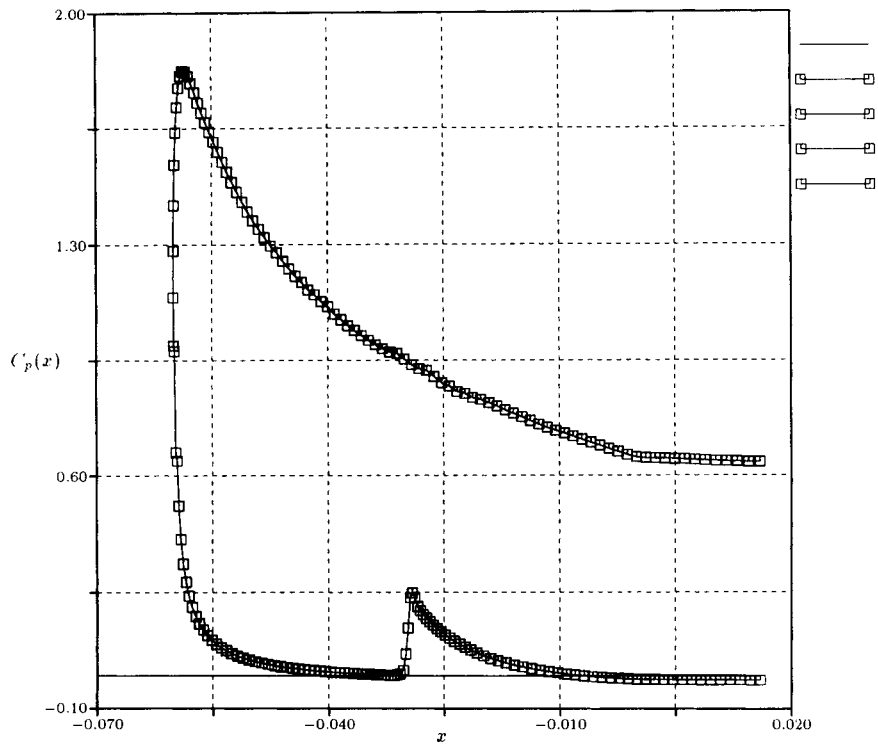

Figure 14. Double ellipse: pressure coefficient distribution along the body

REFERENCES

1. T. J. R. Hughes, 'Finite element methods for fluids', *Proc. AGARD–VKI Lecture Series on Unstructured Grid Methods for Advection Dominated Flows, AGARD Report 787*, 1992.
2. C. Johnson, 'Finite element methods for flow problems', *Proc. AGARD–VKI Lecture Series on Unstructured Grid Methods for Advection Dominated Flows, AGARD Report 787*, 1992.
3. S. K. Aliabadi, S. E. Ray and T. E. Tezduyar, 'SUPG finite element computation of viscous compressible flows based on the conservation and entropy variables formulations', *J. Comput. Mech.*, **11**, 300–312 (1993).
4. T. J. R. Hughes and A. N. Brooks, 'A multidimensional upwind scheme with no crosswind diffusion', in T. J. R. Hughes (ed.), *Finite Element Methods for Convection Dominated Flows*, Vol. 34, ASME, New York, 1979.
5. T. J. R. Hughes, M. Mallet and A. Mizukami, 'A new finite element formulation for computational fluid dynamics: II. Beyond SUPG', *Comput. Methods Appl. Mech. Eng.*, **54**, 341–355 (1986).
6. T. J. R. Hughes and M. Mallet, 'A new finite element formulation for computational fluid dynamics: III. The generalized streamline operator for multidimensional advective–diffusive systems', *Comput. Methods Appl. Mech. Eng.*, **58**, 305–328 (1986).
7. T. J. R. Hughes and M. Mallet, 'A new finite element formulation for computational fluid dynamics: IV. A discontinuity capturing operator for multidimensional advective–diffusive systems', *Comput. Methods Appl. Mech. Eng.*, **58**, 329–336 (1986).
8. C. Johnson, A. Szepessy and P. Hansbo, 'On the convergence of shock-capturing streamline diffusion finite element methods for hyperbolic conservation laws', *Math. Comput.*, **54**, 82–107 (1990).
9. H. Deconinck, 'Beyond the Riemann problem II', *Proc. ICASE–LARC Workshop on Alg. Trends for the 90s*, Hampton, VA, September 1991, Springer, New York, 1992.
10. H. Deconinck, R. Struijs, G. Bourgois and P. L. Roe, 'Compact advection schemes on unstructured grids', *Proc. VKI Lecture Series on Computational Fluid Dynamics, VKI LS 1993-04*, 1993.
11. H. Paillère, H. Deconinck, R. Struijs, P. L. Roe, L. M. Mesaros and J.-D. Müller, 'Computations of inviscid compressible flows using fluctuation-splitting on triangular meshes', *AIAA Paper 93-3301, 1993.*
12. R. Struijs, 'A multi-dimensional upwind discretization method for the Euler equations on unstructured grids', *Ph.D. Thesis*, University of Delft, 1994.

13. H. Paillère, H. Deconinck and A. Bonfiglioli, 'A linearity-preserving wave-model for the solution of the Euler equations on unstructured meshes', *Proc. 2nd Eur. CFD Conf.*, Stuttgart, 1994.
14. P. L. Roe, 'Linear advection schemes on triangular meshes', *COA report 8720*, Cranfield Institute of Technology, 1987.
15. J.-C. Carette, 'Study of the SUPG finite element method for inviscid compressible flows', *Project Report 1993-17*, von Karman Institute, 1993.
16. P. L. Roe, 'Discrete models for the numerical analysis of time-dependent multidimensional gas dynamics', *J. Comput. Phys.*, **63** (1986).
17. H. Paillère, J.-C. Carette and H. Deconinck, 'Multidimensional upwind and SUPG methods for the solution of the compressible flow equations on unstructured grids', *Proc. VKI Lecture Series on Computational Fluid Dynamics, VKI LS 1994-05*, 1994.
18. G. Bourgois, H. Deconinck and P. L. Roe, 'Multidimensional upwind schemes for scalar advection on tetrahedral meshes', *Proc. 1st Eur. CFD Conf.*, Vol. 1 Brussels, September 1992.
19. R. Struijs, H. Deconinck and P. L. Roe, 'Fluctuation splitting schemes for the 2D Euler equations', *Proc. VKI Lecture Series on Computational Fluid Dynamics, VKI LS 1991-01*, 1991.
20. C. Johnson, *Numerical Solution of Partial Differential Equations by the Finite Element Method*, Studentlitteratur, Sweden, 1991.
21. U. Nävert, 'A finite element method for convection–diffusion problems', *Ph.D. Thesis*, Department of Computer Science, Chalmers University of Technology, Göteborg, 1982.
22. H. Deconinck, C. Hirsch and J. Peuteman, 'Characteristic decomposition methods for the multidimensional Euler equations', in *Lecture Notes in Physics*, Vol. 264, Springer, New York, 1986.
23. M. Rudgyard, 'Multidimensional wave decomposition for the Euler equations', *Proc. VKI Lecture Series on Computational Fluid Dynamics, VKI LS 1993-04*, 1993.
24. P. L. Roe, 'Wave-modelling of time-dependent hyperbolic systems', *ICASE Report*, 1994.
25. P. Roe, R. Struijs and H. Deconinck, 'A conservative linearization of the multidimensional Euler equations', *J. Comput. Phys.*, in press.
26. P. Hansbo, 'Explicit streamline diffusion finite element methods for the compressible Euler equations in conservation variables', *J. Comput. Phys.*, **109**, 274–288 (1993).
27. H. M. Glaz and A. B. Wardlaw, 'A high-order Godunov scheme for steady supersonic gas dynamics', *J. Comput. Phys.*, **58** (1985).
28. J.-D. Müller, P. L. Roe and H. Deconinck, 'Delaunay-based triangulations for the Navier–Stokes equations with minimum user input', in *Lecture Notes in Physics*, Vol. 414, Springer, New York, 1992.
29. R. Richter, Schèmas de capture de discontinuitès en maillage non-structurè avec adaptation dynamique. Applications aux ècoulements de l'aèrodynamique', *Ph.D. Thesis*, IMHEF, Ecole Polytechnique Fédérale de Lausanne, 1993.
30. 'Numerical simulation of compressible Euler flows', in A. Dervieux, B. van Leer, J. Periaux and A. Rizzi (eds.), *Notes on Numerical Fluid Mechanics*, Vol. 26, Vieweg, Braunschweig, 1989.
31. P. Roe and L. Beard, 'An improved wave model for multidimensional upwinding of the Euler equations', *Proc. 13th Int. Conf. on Numerical Methods in Fluid Dynamics*, Rome, July 1992.
32. M. Giles, W. Anderson and T. Roberts, 'Upwind control volumes: a new upwind approach', *AIAA Paper 90-0104*, 1990.
33. 'Hypersonic flows for reentry problems', in J.-A. Desideri, R. Glowinski and J. Periaux (eds.), *Proc. Workshop*, Antibes, January 1990, Vol. II, Springer, New York 1991.